Available online at www.sciencedirect.com
SCIENCE DIRECT
Journal of Power Sources 151 (2005) 43–51
JOURNAL OF POWER SOURCES
www.elsevier.com/locate/jpowsour

Cerium–terbium mixed oxides as potential materials for anodes in solid oxide fuel cells

A. Martínez-Arias [a], A.B. Hungría [a], M. Fernández-García [a], A. Iglesias-Juez [a], J.C. Conesa [a,*], G.C. Mather [b], G. Munuera [c]

[a] *Instituto de Catálisis y Petroleoquímica, CSIC, c/Marie Curie, Campus Cantoblanco, 28049 Madrid, Spain*
[b] *Instituto de Cerámica y Vidrio, CSIC, Camino de Valdelatas s/n, Campus de Cantoblanco, 28049 Madrid, Spain*
[c] *Departamento de Química Inorgánica, Universidad de Sevilla, 41092 Sevilla, Spain*

Accepted 4 February 2005
Available online 26 April 2005

Abstract

Highly homogeneous (Ce,Tb) oxides are prepared by a microemulsion technique, and their structural and electronic state after high temperature calcination is examined with X-ray diffraction, high resolution transmission electron microscopy, X-ray photoelectron and absorption (XANES) spectroscopies and impedance spectroscopy measurements. Addition of Tb stabilizes significantly (in comparison to pure ceria) specific surface area and small particles sizes during high temperature calcination (up to 1100 °C); phase decomposition at these high temperatures, similar to that occurring when stabilization of ceria is carried out with Zr, does not occur, and the mixed oxide remains homogeneous throughout. Tb addition to ceria may thus be beneficial when used as a component of SOFC anodes. TEM data indicate reshaping of oxide particles and provide evidence of crystal superstructures after high temperature treatments, while XPS and XANES reveal an increase in the Tb^{4+}/Tb^{3+} ratio (for a given pretreatment) with the Tb/Ce ratio; Ce seems to be less reducible to Ce^{3+} in the presence of Tb. Total electrical conductivity of CT samples under H_2 is mediated by electron transport (involving probably only Ce) and is lower than in gadolinia-doped ceria (GCO); in air conductivity is higher than for GCO, particularly at low temperatures, and it is probable that a p-type transport mechanism predominates in this case.

Keywords: Cerium oxide; Terbium oxide; Solid oxide fuel cell; Anode; Structure; Surface area

1. Introduction

The use of ceria in Solid Oxide Fuel Cell (SOFC) anodes has received attention in recent years, particularly after the work by Park et al. [1], which shows its beneficial effect when the anode is fed directly with dry hydrocarbon as fuel; this is thought to be related to the known good characteristics of ceria as catalyst for the total oxidation of hydrocarbons. In these conditions of direct dry hydrocarbon feed, there is the problem that the Ni metal component used as electrical conductor in the anode composite promotes the formation of carbon, which decreases the anode efficiency by blocking its pores. This has led some authors to propose the use in the anodes of copper, which is much less prone than nickel to promote carbon formation [2]. Copper has, however, the disadvantage of a lower melting point which leads to its gradual particle growth during cell operation, this being ultimately detrimental to the necessary electrical conduction. For this reason, Kim et al. [3] have proposed using a Ni–Cu alloy; this not only retards the metal particle growth but also gives rise to the formation of a small amount of carbon that, if adequately controlled, does not block pores and contributes to the required electronic conductivity; the amount of metal can, thus, also be lowered, allowing better control of particle size. This approach may require, however, a delicate control of material properties and process parameters to ensure that

* Corresponding author. Tel.: +34 91 5854766; fax: +34 91 5854760.
E-mail addresses: jcconesa@icp.csic.es (J.C. Conesa), mather@icv.csic.es (G.C. Mather), munuera@us.es (G. Munuera).

0378-7753/$ – see front matter © 2005 Elsevier B.V. All rights reserved.
doi:10.1016/j.jpowsour.2005.02.079

the amount and characteristics of the formed carbon remain stable within the desired limits. Tuning of the properties of the ceria component will be important also in this respect. It may be mentioned here that other approaches to avoid carbon formation have been proposed, as e.g. using redox-active perovskites [4,5] or Pt as conducting metal [6]. Those other kinds of approaches are not addressed in this work.

One of the issues here is related to the stability of the anode materials. In this respect, it is important to keep an adequate surface area in the oxide component of the anode composite, in order to enhance its catalytic properties. The hydrocarbon oxidation catalyst, ceria, has the disadvantage of being less refractory than the zirconia-based materials typically used in SOFC anodes, and can therefore undergo heavier sintering and loss of surface area during cell manufacture and operation. One way to counteract this could be to add an element to ceria such as Zr, which has proven very useful in this respect in stabilizing ceria in automobile exhaust gas catalytic converters [7]; however, Zr–Ce mixed oxides are known to decompose in phases of mainly ceria and mainly zirconia composition when treated at temperatures above 1000 °C, which may lead to mechanical instabilities so that their use in SOFC, which may easily reach such temperatures during their manufacture, would not be recommended.

In the present work, the alternative is explored of using Tb instead of Zr as stabilizing additive to ceria. Tb^{4+} has ionic radius smaller than that of Ce^{4+} (so that a stabilization of a small ceria particle size is expected, and indeed, it has been verified for temperatures below 900 °C [8]), but larger than that of Zr^{4+}, so that incompatibilities with the ceria lattice will be lower (indeed TbO_2 has a cubic fluorite structure) and one may thus expect that such a decomposition will not take place.

In addition, Tb easily presents a mixture of valence states (Tb^{4+} and Tb^{3+}). This may be beneficial for anode operation in two respects. First, this might provide a path, based on electron transfer between both states, for better electron transport, particularly at the microscopic level, between the oxide and the metal (or carbon) conductor in the anode composite. This may facilitate the overall electrochemical process and make it perhaps less critically dependent on the structure of the carbon conductor component when this latter is desired as in the case mentioned above. Such electron transport by the oxide component is present as well when perovskites are used, as in the mentioned Refs. [4,5]. Additionally, the presence of a second redox couple in the oxide (Tb^{4+}/Tb^{3+} besides Ce^{4+}/Ce^{3+}) may provide additional pathways for redox reactions at the anode surface, facilitating its catalytic action for hydrocarbon oxidation. Finally, the terbium ion, in the reduced state Tb^{3+}, has an ionic radius close to that of Gd^{3+}, and thus, one may expect that it could contribute to the ionic conductivity of the oxide, and be beneficial also for the anode operation in this respect.

Within this perspective, the present work focuses on the structure and redox state of mixed oxides of Ce and Tb, considering mainly the macroscopic behaviour of the material (surface chemical properties will be the subject of a separate study), exploring pretreatment temperatures not reached in our previous work and characterizing the materials with several techniques to understand the extent and nature of the mixing and relative interactions between both Ce and Tb components.

2. Experimental

The mixed oxides were prepared through a microemulsion-based method, described elsewhere [9,10]. Briefly, an inverse microemulsion, containing a solution of appropriate amounts of the metal nitrates as aqueous phase in its small surfactant-stabilized droplets, was mixed with another similar microemulsion in which the aqueous component was a tetramethylammonium hydroxide solution. Upon mixing, oxides precipitated inside the aqueous droplets, and after stirring the solid formed was separated, rinsed and calcined in air, initially at 500 °C. Samples with nominal Ce:Tb atomic ratios equal to 4 and 1 were thus made, labeled hereafter as CT4 and CT1, respectively (actual Ce:Tb ratios obtained were 3.93 and 1.10 according to chemical ICP-AES analysis). For comparative purposes, pure Ce and Tb oxides were prepared by a similar method, and are labeled C and T, respectively. Subsequent calcinations were carried out as needed at higher temperatures T_c of 900 and 1100 °C (and 1500 °C in some sintering treatments necessary for electrical conductivity measurements). Where appropriate, the calcination temperature values are indicated appended to the composition labels. The prepared materials were characterized with several techniques. BET specific area measurements (S_{BET}) were carried out with a Micromeritics ASAP 2010 system. X-ray diffraction (XRD) was conducted with a Seifert XRD 300P diffractometer using Ni-filtered Cu Kα radiation and operating at 40 kV and 40 mA.

Transmission electron microscopy (TEM) data of low temperature calcined samples were obtained in a JEOL 2000 EX microscope with 0.21 nm point to point resolution, equipped with a top entry specimen holder; the experimental micrographs were digitized using a COHU-4910 CCD camera. X-ray energy dispersive spectroscopy (XEDS) analyses were carried out using a JEOL 2000 FX system equipped with a LINK (AN 10000) probe; sample spot for XEDS analysis is about 100 nm. TEM data of sintered samples were acquired with a field electron gun Philips CM200 microscope, with 0.24 nm point to point resolution, equipped with a XEDS EDAX DX4 detector; sampling spot size is in this latter case about 20 nm.

X-ray photoelectron spectra (XPS) were recorded with a Leybold–Heraeus spectrometer equipped with an EA-200 hemispherical electron multichannel analyzer (from Specs) and a 120 W, 30 mA Al Kα X-ray source. Depth profiles of the near-surface regions could be obtained through sputtering with Ar^+ ions using a current of 6 mA and an acceleration voltage of 3.5 kV (ion current, 8 μA). The sample (0.2 g) was

slightly pressed into a small (4 mm × 4 mm) pellet and then mounted on a sample rod and introduced into the pretreatment chamber where it was outgassed at 473 K for 2–3 h, until a pressure of less than 2×10^{-8} Torr was achieved; thermal treatments under H_2 or O_2, followed by outgassing, were carried out in the same pretreatment chamber as required. The spectrum intensities were estimated by calculating the integral of each peak after subtraction of an S-shaped Shirley-type background with the help of UNIFIT for Windows (Version 3.2) software [11]; atomic ratios were then derived using the appropriate experimental sensitivity factors. All binding energies (BE) were referenced to the adventitious C1s line at 284.6 eV. This reference gave BE values with an accuracy of ±0.1 eV; the peak u''' characteristic of Ce^{4+} was thus obtained at 917.0 ± 0.1 eV. In the case of the Tb(3d) spectra, factor analysis (also known as principal component analysis) was used to calculate the Tb^{3+}/Tb^{4+} ratios in each set of spectra recorded, using the methodology developed in a previous work [12].

X-ray absorption near edge spectroscopy (XANES) was carried out in transmission mode in station 9.3 at the SRS synchrotron in the Daresbury Laboratory (Warrington, UK), using a Pd-coated plane mirror and a Si(2 2 0) double crystal monochromator with 50% harmonic rejection detune. Two ionization chambers filled with N_2/O_2 and self-supported sample pellets with an absorbance below 1.5 were used in the measurements.

Impedance spectroscopy (IS) measurements were carried out on samples sintered at 1500 °C for 12 h in order to minimise grain-boundary contributions in the determination of the total conductivity. X-ray diffraction of the sintered pellets confirmed the presence of single phase fluorite-type material at XRD resolution, as observed for the lower temperature treatments. For conductivity measurements, the sintered pellets were coated with Pt paste (SPI Supplies) and fired at 700 °C for 1 h to remove the organic content. Impedance spectroscopy was performed with an Agilent 4294A instrument in the range $40 \leq f \leq 5 \times 10^6$ Hz, computer controlled with the Sweep software [13]. Data were collected in the temperature range 400–800 °C in air and under a flow of a H_2:N_2 mixture bubbled through water and fed to the chamber at a rate of 50 ml min^{-1}. Measurements were taken on cooling in steps of 50 °C allowing at least 50 min for thermal equilibrium to be established. On changing atmosphere, data were collected after a period of at least 12 h or once steady-state had been reached. Data were also obtained as a function of $p(O_2)$ by first equilibrating the furnace in reducing atmosphere, then switching off the gas flow and allowing the $p(O_2)$ to rise through the slow leakage of oxygen into the furnace. The $p(O_2)$ was monitored with an yttria-stabilized ZrO_2 (zirconia) sensor placed adjacent to the sample and attached with Pt electrodes to an external voltmeter. Analysis of spectra was conducted with the ISA program [14] and fitted with the EQUIVCRT program [15].

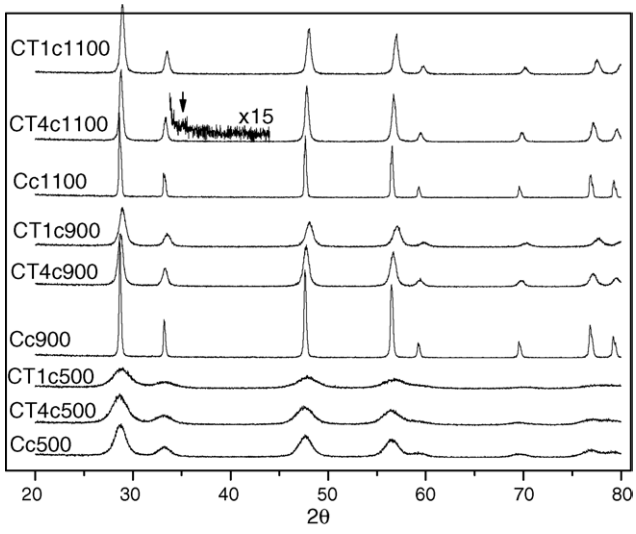

Fig. 1. XRD profiles of the studied samples. The arrow in the amplified range of CT4-1100 sample marks a peak possibly corresponding to a lattice superstructure.

3. Results and discussion

3.1. Structural analysis

The initial samples (calcined at 500 °C) present high S_{BET} area (Table 1). Their XRD profiles (Fig. 1) correspond to the fluorite lattice, with unit cell parameters varying with Tb content (Table 1), and show broadened lines indicating small particle sizes below 10 nm. These small particle sizes are confirmed by TEM measurements; the obtained micrographs (Fig. 2) clearly reveal fluorite structure fringes, in agreement with the diffraction patterns (see inset in the figure), while XEDS shows throughout a homogeneous distribution of Ce:Tb ratios.

After calcination at 900 or 1100 °C, a substantial improvement in crystallinity is observed, as expected (see diffractograms in Fig. 1), with corresponding increase in crystallite size and decrease in specific surface area (Table 1). It is worth

Table 1
Specific area (S_{BET}) and fluorite cell parameter (XRD) of the ceria and ceria–terbia samples

	Sample								
	C-500	CT4-500	CT1-500	C-900	CT4-900	CT1-900	C-1100	CT4-1100	CT1-1100
S_{BET} (m^2 g^{-1})	115	146	111	2	20	8	<0.5	8	4
a (Å)	5.412	5.412	5.391	5.410	5.396	5.365	5.405	5.392	5.374

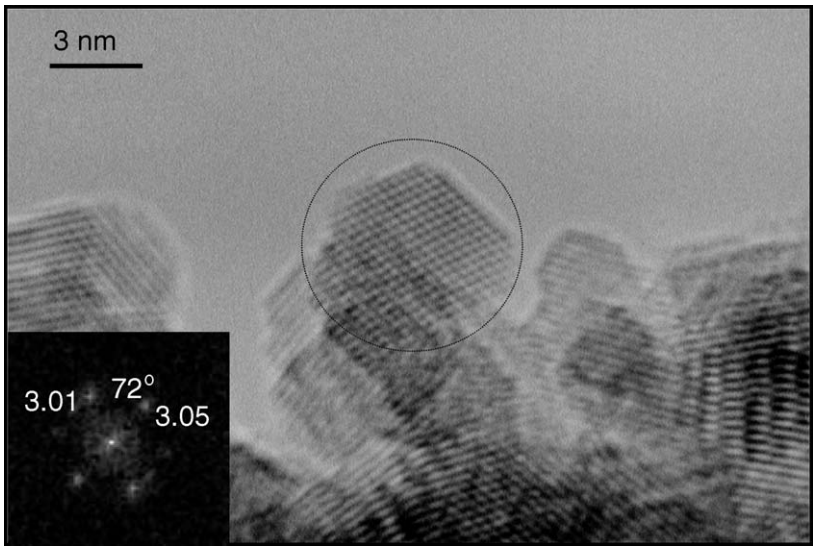

Fig. 2. Representative TEM micrograph of sample CT4 (calcined at 500 °C). The digital diffraction pattern shown corresponds to the indicated particle and is typical of fluorite structure.

remarking here that a demixing of the mixed oxide in two phases with different cation ratios and cell parameters, as occurs for $(Ce,Zr)O_2$ upon high temperature treatment [16], has not been observed in the present study. The decrease in S_{BET} is lower for the Tb-containing samples, but this sintering retardation effect is larger in sample CT4 than in sample CT1. This indicates that already from the structural point of view Tb may be beneficial to obtain a ceria phase with high surface area as required in SOFC anodes (provided sufficient development of inter-grain connectivity for electrical and chemical transport occurs). This is probably due to the smaller radius of the Tb ion compared to Ce (for both 3+ and 4+ Tb redox states). The data also show that the surface area does not increase monotonously with Tb content; instead, it seems that there is an optimum Tb:Ce ratio, the value of which remains to be established. The reason for this non-monotonous behavior is not clear, but some indication is provided by TEM data as shown below.

On the other hand, a decrease in cell parameter with increasing Tb fraction, which was also observable in the materials calcined at 500 °C, appears more markedly for the samples calcined at higher temperatures. Tb^{3+} has an ionic radius similar to that of Ce^{4+} (the fluorite-related structure of cubic Tb_2O_3 has a cell parameter just 0.85% smaller than that of CeO_2 [17]), whereas that of Tb^{4+} is much lower (TbO_2 has unit cell constant $a = 5.213$ Å [18], 3.7% lower). Hence, the significantly lower cell constant of Tb-containing phases with respect to CeO_2 is interpreted as due to the presence of Tb^{4+} (an effect of small crystallite size on cell constant would be plausible only for much smaller particles). The further decrease (within each Tb concentration) observed after high temperature calcination implies an increase of the ratio $f(Tb^{4+}) = Tb^{4+}/(Tb^{3+} + Tb^{4+})$, although increasing T_c from 900 to 1100 °C does not always cause this effect. This overall variation is contrary to what one would expect in such oxides from thermodynamics, according to which higher temperatures would cause, if anything, a decrease in both the oxygen content and this ratio. The probable reason must, therefore, be kinetic in nature, i.e. the high temperature favours a faster ion diffusion and equilibration of the samples with air (which initially have substantial amounts of Tb^{3+}, probably due to the adopted precipitation method).

TEM micrographs of the mixed oxide samples calcined at 900 and 1100 °C (Fig. 3) show an increase in crystallite size with T_c as observed by XRD. A particularly evident difference between CT1 and CT4 samples is that the former present a much more agglomerated microstructure, which explains their lower S_{BET} (the difference in crystallite sizes between both specimens for each T_c is, according to the micrographs, much less marked). It seems, thus, that at high temperatures CT1 has a significantly higher overall ion mobility than CT4, which facilitates coalescence. This might be due to a higher lattice strain [8], associated with the ionic radius mismatch and/or to a higher concentration of anion vacancies; its destabilizing effect on the crystalline lattice could overcome the effect of the Madelung energy increase arising from the smaller cation radius. Greater sintering of particles may increase conductivity and interparticle transfer of chemical species, an advantage which might compensate to some extent the negative effect of the lower surface area on anode operation.

For the less agglomerated CT specimens, TEM occasionally shows double periodicities in the micrographs: the digital diffraction patterns show dots corresponding to spacings of 5.2 and 4.3–4.4 Å that do not appear for the fluorite structure (Fig. 4A). Simulations indicate that these features may appear for a superstructure with doubled cell constant and cubic space group Ia-3 (or its $I2_13$ subgroup), i.e. consistent with the bixbyite structure of the sesquioxides of lanthanides with $Z \geq 62$. In the XRD patterns, reflections correspond-

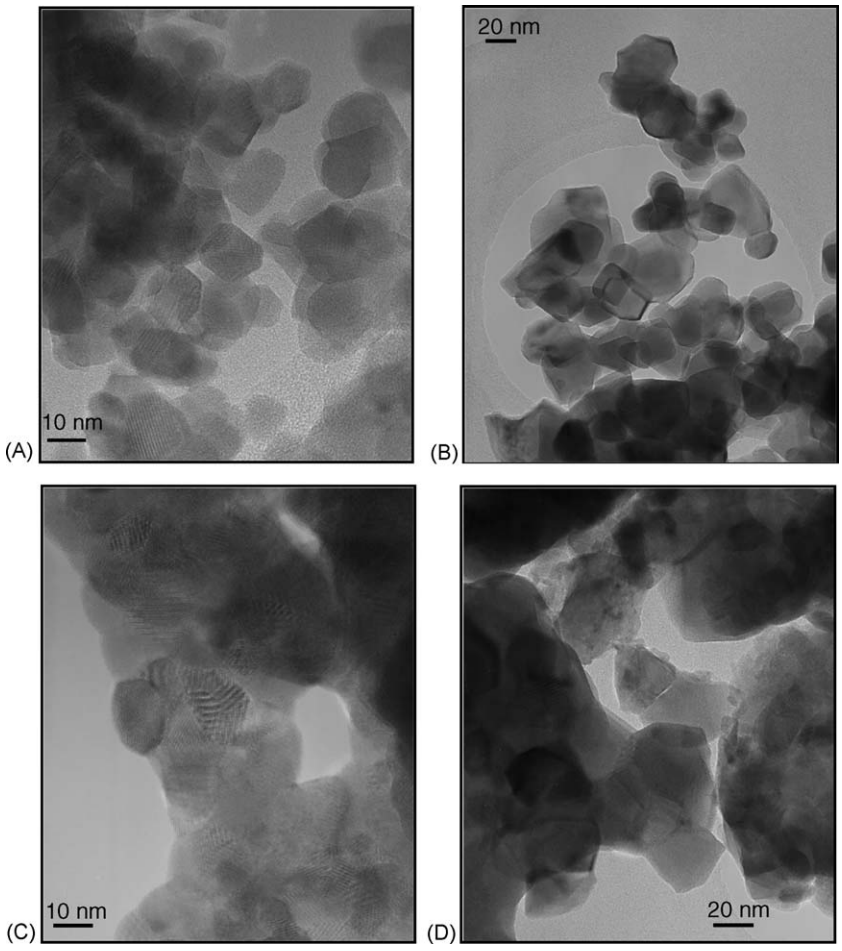

Fig. 3. Electron micrographs of mixed oxide samples calcined at high temperature: (A) CT4-900, (B) CT4-1100, (C) CT1-900, (D) CT1-1100.

ing to such a superstructure were not observed, except for a faint feature at 35.1° discerned for specimen CT4-1100 (see Fig. 2). This could correspond to the (4 1 1) reflection in a doubled cell belonging to one of these space groups. This superstructure results through anion vacancy ordering, and has been detected with XRD even in pure ceria when reduced at temperatures too low to allow the formation of the stable hexagonal Ce_2O_3 phase [19]. The extra diffraction spots and superlattice fringes were shown by TEM for both CT4 and CT1 samples sintered at 900–1000 °C, but the XRD patterns only revealed superstructure features for CT4-1100, suggesting a less extensive ordering in the other samples. There is no clear explanation yet for the fact that supercell formation was not observed by XRD for the CT1 materials, in spite of the fact that the higher amount of Tb is expected to increase the concentration of vacancies.

It may also be indicated here that the crystallite shapes observed in the materials calcined at 900–1100 °C were appreciably different from those usually seen in previous works for ceria or ceria–zirconia specimens [20], also calcined at high temperatures. In those cases, cuboctahedral shapes were clearly dominant (see as an example Fig. 4B), while here near-rectangular profiles were also frequent, indicating a higher occurrence of (1 0 0)-plane terminations. It is known that of CeO_2 the most stable exposed surfaces are (1 1 1) and (1 1 0) [21], while the (1 0 0) surface needs a substantial number of anion vacancies to be stabilized. It may be that the number of vacancies present, at least at the surface, during the high temperature treatment in the Tb-containing samples may allow such (1 0 0) surfaces to stabilize leading to the observed particle shapes, which would remain unchanged when quenching the specimens to room temperature. This should be taken into account when analyzing the surface reactivity of these materials, which may become modified to some extent if the crystal plane which is preferentially exposed changes. In this respect, it is worth mentioning that for ceria-type oxides treated at high temperatures, a change in surface reactivity was observed, which, for a given outgassing treatment, generated a greater concentration of anion vacancies on the surface than found for specimens treated at lower temperatures [22].

3.2. Spectroscopic data

The redox state of the cations in the specimens was examined with XANES spectroscopy. Data obtained at the Ce L_{III} absorption edge (not shown) indicated a dominant Ce^{4+} state

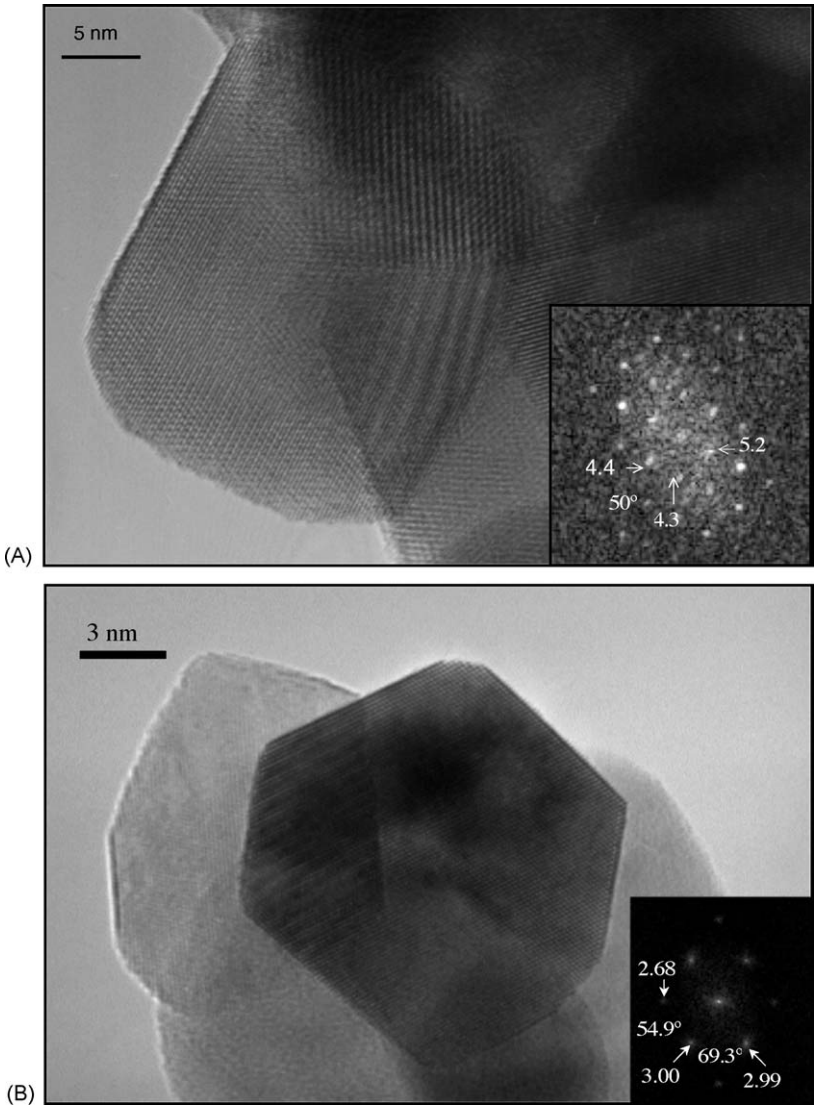

Fig. 4. High resolution micrographs of high-temperature treated materials. (A) sample CT4-1100. The central crystallite shows additional periodicity features in respect to the fluorite lattice fringes, also indicated by the new spots in the digital diffraction pattern shown in the inset. (B) Typical crystallite of a $CeZrO_4$ material prepared by the same method and calcined at 1000 °C (from Ref. [20]), shown for comparison.

in all mixed oxide samples. On the other hand, the spectra at the Tb_{III} edge (Fig. 5) varied significantly with composition and T_c. As in the better known case of Ce, the terbium L_{III} XANES spectrum shows one main peak just at the edge (a "white line") when in the Tb^{3+} state (as observed in other typically trivalent lanthanide oxides), while in the Tb^{4+} state a splitting appears which is normally ascribed to the presence of mixed configuration effects in the ground state leading to two main excitation channels (with and without transfer of one electron from the oxygen ligands to the 4f levels) in the $2p \rightarrow 5d$ transition responsible for this line [23]. In a system containing both Tb^{4+} and Tb^{3+}, the intensity ratio between the two peaks is a measure of the proportion of both states, and although the calibration data necessary for obtaining absolute $f(Tb^{4+})$ values are lacking here, it is possible to conclude from the spectra that this fraction appears to be minimum in CT4 calcined at 500 °C and maximum for pure TbO_x calcined at the higher temperatures, i.e. the Tb^{4+} content increases with T_c and with the Tb/Ce ratio, as was deduced from the XRD data.

XPS measurements can provide information on the concentration and degree of oxidation of the cations in the surface regions of these materials (photoelectrons escape depths are ca. 6 and 11 Å for Tb and Ce, respectively, and consequently the total depths actually probed are correspondingly ca. 20 and 35 Å). Such data could be measured for some of these samples (see Fig. 6). The surface Tb/Ce ratios were measured to be 0.45 and 0.18 for CT1 and CT4, respectively; these values are very close to the bulk composition and do not change appreciably after Ar^+ sputtering, indicating a high degree of homogeneity of the materials, without significant surface enrichment in either element. For TbO_x, the Tb 3d spectra

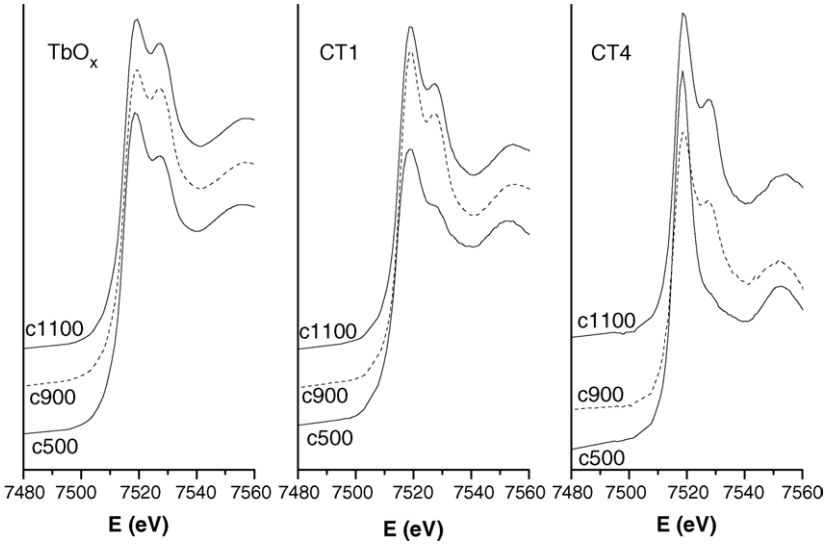

Fig. 5. XANES spectra in the Tb L_{III} edge for the different Tb-containing samples.

(Fig. 6b) show that the Tb^{4+} state manifests itself through satellites with binding energy ca. 10 eV higher than those of the main peaks (with $E_B = 1241.3$ eV for the $3d_{5/2}$ component of the doublet); rigorous examination revealed that the position and shape of the main peaks of both redox states in these oxides are practically indistinguishable, contrary to earlier reports [24]. The proportion of +3 and +4 states can, therefore, be obtained through Principal Component Analysis (PCA) provided that the spectrum of Tb^{4+} can be isolated [25]. Assuming that the spectrum of TbO_x oxidized at 500 °C (in Fig. 6b) corresponds mainly to Tb^{4+} (which is supported by the fact that the O/Tb surface atomic ratio measured by XPS in this case is O/Tb ≈ 2.2), a tentative analysis indicates that for the samples CT1 (Fig. 6a) and CT4 (rather similar in appearance, not shown) calcined at 500 °C, pretreated in the spectrometer in vacuo at 200 °C to clean the surface, the outer regions have $f(Tb^{4+})$ values of 0.60 and 0.35, respectively. It is noteworthy that in these experiments the Ce 3d spectra (not shown) revealed the almost exclusive presence of Ce^{4+}, while pure ceria treated in similar conditions exhibits significantly higher amounts of Ce^{3+}; this indicates that upon moderate reduction of these materials, the excess electrons are located on Tb in preference to Ce. This is not surprising since Tb oxide is known to adopt the trivalent state much more easily than Ce (indeed fully oxidised stoichiometric TbO_2 is notoriously difficult to prepare [26], and commercial oxides of Tb normally have a stoichiometry close to $TbO_{1.7}$). The results also confirm the general trend observed above with XANES for the bulk of the oxide, but now at the surface level, in the sense that, for any given pretreatment, the average oxidation state of Tb in these oxides increases with Tb/Ce ratio.

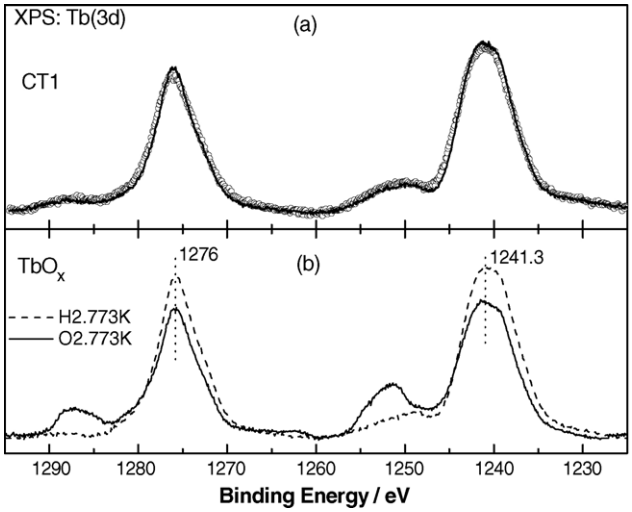

Fig. 6. XP spectra, in the Tb 3d range, for some of the samples examined. Lower part: spectra for pure TbO_x oxidized (in O_2) and reduced (in H_2) at 500 °C within the spectrometer pretreatment chamber. Upper part: experimental spectrum for the CT1 sample (small circles) compared with the sum of Tb^{3+} (40%) and Tb^{4+} (60%) contributions (full line) resulting from Principal Component Analysis.

3.3. Electrical properties

Some preliminary electrical conductivity data were obtained for the mixed oxide specimens and are reported here. The attention at this stage was focused on the macroscopic electrical properties of the oxides to assess the behaviour of the materials for the current-carrying role of the anode. The influence of other anode characteristics, which may contribute to a desirable low polarisation resistance, such as a suitably large surface area and most effective composition for efficient electrocatalytic oxidation of the fuel, were not addressed in this work. In order to minimise the grain-boundary contribution to the impedance, measurements were performed on pellets sintered at 1500 °C in air. The total conductivities as a function of temperature obtained for CT1 and

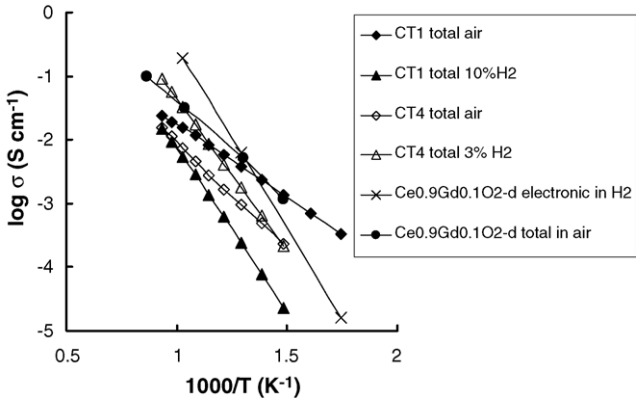

Fig. 7. Total conductivity data of CT samples (sintered in air at 1500 °C) obtained in air and reducing conditions. The data for $Ce_{0.9}Gd_{0.1}O_{2-\delta}$ are taken from Refs. [27,28].

CT4 both in air and under humidified H_2:N_2 mixtures are presented in Fig. 7. Also shown are data for standard GCO (10% Gd) [27,28], which correspond to the total conductivity in air and the electronic contribution to the total conductivity in hydrogen. In reducing atmosphere, the total conductivity of CT1 is ca. one order of magnitude lower than the electronic (n-type) component of the conductivity of GCO; that for CT4 was higher (in slightly less reducing conditions) although still lower than that of GCO. All three compositions (in reducing atmosphere) display a practically identical slope in the Arrhenius plots, with apparent activation energy of 1.08 eV. For CT1, the dependence of the conductivity on oxygen partial pressure $p(O_2)$ was determined at 650 °C (Fig. 8), and revealed a $p(O_2)^{-1/4}$ relationship for $p(O_2) < 10^{-21}$ atm., in accordance with a −1/4 power law characteristic of n-type conductivity. Hence, to a first approximation, the increase in conductivity with increasingly reducing atmosphere (below $p(O_2) < 10^{-21}$ atm) may be assumed to arise mainly from reduction of the sample to form mobile electrons whereas the oxide-ion vacancies with much lower mobility, which are concomitantly formed on reduction, may be considered to have an insignificant contribution to the enhanced conductivity. We note, however, that the resolution of the conductivity

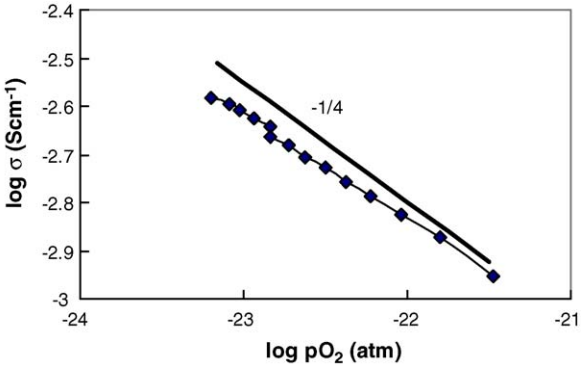

Fig. 8. Plot of total conductivity vs. $\log p(O_2)$ for CT1 sample at 650 °C.

into the different charge-carrier contributions has not been fully conducted at this stage.

The fact that the activation energy in these CT samples under reducing conditions is, within experimental uncertainty, the same as in GCO, strongly suggests that the conduction mechanism is also the same, i.e. that electron (small polaron) hopping takes place between Ce^{3+} and Ce^{4+} species and that Tb ions contribute to a much lower extent. This can be understood considering the previous discussion of the greater reducibility of Tb in comparison to Ce: it is likely that in these highly reducing conditions the great majority of Tb ions exist as Tb^{3+}, decreasing the availability of sites for electron hopping between Tb ions, while on the other hand jumps from Tb^{3+} to Ce^{4+} will be unfavourable due to the clearly higher stability of the Tb reduced state in comparison to that of Ce. Thus, Tb would not contribute substantially to electron transport across the solid in these conditions. Additionally, the lower absolute conductivity in the Ce–Tb oxides with respect to GCO (electronic component) is probably also due to a smaller concentration of Ce^{3+}, which tends to be lower in the presence of Tb as discussed earlier.

It is apparent that Tb inclusion does not enhance the conductivity on the macroscopic level in reducing conditions and one could infer that the CT materials would not, therefore, be suitable for the current-carrying function of the anode. However, when accompanied by a suitably conductive oxide or metallic phase in the anode, the properties of the title materials may be of interest for the following reasons. The present conductivity data provide no information on the behaviour of the surface regions where electrocatalytic oxidation takes place, in a porous anode. Although the fuel fed to the anode in real SOFC operation (be it H_2, CO, natural gas or other hydrocarbon) is a strong reductant, the anode is also subjected to localised oxidising phenomena, especially at the anode/electrolyte interface, and is not therefore at equilibrium with the gas atmosphere over the entire anode surface. In the stationary state at least, some regions may be significantly more oxidised than when just in contact with H_2. Hence, at the local level, there might be a significant amount of Tb^{4+} which could participate in electrocatalytic activity through Tb^{3+}/Tb^{4+} redox couples, in addition to that provided by Ce^{3+}/Ce^{4+} couples, and which might result in a more effective oxidation than that achieved with standard gadolinium-doped ceria.

In fact, the conductivity of the CT1 sample in air is significantly higher than that of GCO (Fig. 7) in the low temperature range with a smaller activation energy (0.52 eV) in comparison to GCO [28]. This implies that the conduction mechanism is not the same as in reducing conditions (so that the same dependence on $p(O_2)$ found under reducing conditions cannot be extrapolated to the situation under air). It is highly likely that in the oxidising conditions Tb ions instead mediate the electron jump (i.e. between Tb^{4+} and Tb^{3+}) in accordance with a p-type transport. The effective redox conditions affecting the material in the dynamic conditions of real cell operation are difficult to determine and will need

more extensive studies. Nevertheless, the data suggest that Tb doping could be a relevant parameter for SOFC anode operation, at least at a local level, in the regions closest to the electrolyte, especially in the lower temperature range. Further experiments to clarify this aspect are in progress.

4. Conclusions

The preparation via a microemulsion method of mixed Ce, Tb oxides leads to materials which maintain their high compositional homogeneity after air-calcination temperatures up to 1100 °C (in contrast to Ce, Zr mixed oxides). In addition, the retention of a moderately high surface area is significantly better with respect to pure ceria in the same conditions, especially for moderate amounts of Tb. Thus, from this point of view, inclusion of Tb in ceria may be a positive factor when the latter is used in SOFCs as anode electrocatalytic material. For high Tb content, crystallite sizes remain relatively small, but important agglomeration occurs that significantly decreases the exposed surface area.

High temperature calcination leads not only to an increase in the size of crystallites but also to some structural rearrangements which induce changes in the crystallite shape; this might be due to a different relative stability of different exposed crystal planes under the calcination conditions. HR-TEM data suggest the onset of anion vacancy and/or cation ordering in the high temperature calcined materials.

In the calcined oxides, moderate reduction primarily involves the Tb species; the reduction of Ce may thus be retarded in comparison with the situation for pure CeO_2. Furthermore, XANES data indicate that the Tb^{4+}/Tb^{3+} ratio increases with the Tb/Ce ratio, in agreement with previous data on similar materials calcined at lower temperatures.

Accordingly, electrical conductivity is lower for the title phases than for GCO in reducing conditions, most probably due to the prevalent reduction of Tb to the Tb^{3+} state and the lower concentration of Ce^{3+} (n-type) charge carriers. However, there may be advantageous effects of the Tb^{4+}/Tb^{3+} redox couple at the anode surface in real anodic conditions, especially where local oxygen chemical potential gradients arise close to the anode–electrolyte interface.

Acknowledgements

Thanks are given to CICYT (Project MAT2003-03925) for financial support of this research, to the Universities of Madrid (Complutense) and Cádiz for the facilities given for the obtention of TEM data, to ICP-Unidad de Apoyo staff for chemical analysis results and XRD recording, to technical staff at Daresbury Laboratory Station 9.3 (Drs. I. Harvey and A.R. Lennie) for the help given during recording of the XAFS spectra, and to Mr. A. Macías for assistance in recording the XPS data.

References

[1] S. Park, R. Craciun, J.M. Vohs, R.J. Gorte, J. Electrochem. Soc. 146 (1999) 3603.
[2] R.J. Gorte, S. Park, J.M. Vohs, C. Wang, Adv. Mater. 12 (2000) 1465.
[3] H. Kim, C. Lu, W.L. Worrell, J.M. Vohs, R.J. Gorte, J. Electrochem. Soc. 149 (2002) 247.
[4] S.W. Tao, J.T.S. Irvine, Nat. Mater. 2 (2003) 320.
[5] D.P. Fagg, V.V. Kharton, A.V. Kovalevsky, A.P. Viskup, E.N. Naumovich, J.R. Frade, J. Eur. Ceram. Soc. 21 (2001) 1831.
[6] S. Tao, J.T.S. Irvine, J. Electrochem. Soc. 151 (2004) 497.
[7] M. Shelef, G.W. Graham, R.W. McCabe, in: A. Trovarelli (Ed.), Catalysis by Ceria and Related Materials, Imperial College Press, London, 2002, p. 343.
[8] X. Wang, J.C. Hanson, G. Liu, J.A. Rodríguez, A. Iglesias-Juez, M. Fernández-García, J. Chem. Phys. 121 (2004) 5434.
[9] A. Martínez-Arias, M. Fernández-García, V. Ballesteros, L.N. Salamanca, J.C. Conesa, C. Otero, J. Soria, Langmuir 15 (1999) 4796.
[10] A.B. Hungría, A. Martínez-Arias, M. Fernández-García, A. Iglesias-Juez, A. Guerrero-Ruiz, J.J. Calvino, J.C. Conesa, J. Soria. Chem. Mater. 15 (2003) 4309.
[11] R. Hesse, T. Chassé, R. Szargan, Fresenius J. Anal. Chem. 365 (1999) 48.
[12] J.P. Holgado, R. Alvarez, G. Munuera, Appl. Surf. Sci. 161 (2000) 164.
[13] J.C.C. Abrantes, Sweep Control, Polytechnic Institute of Viana do Castelo, Portugal, 2003.
[14] J.C.C. Abrantes, ISA-Impedance Spectroscopy Analysis, Polytechnic Institute of Viana do Castelo, Portugal, 2003.
[15] B.A. Boukamp, Solid State Ionics 20 (1986) 31.
[16] H.W. Jen, G.W. Graham, W. Chun, R.W. McCabe, J.P. Cuif, S.E. Deutsch, O. Touret, Catal. Today 50 (1999) 309.
[17] A. Saiki, N. Ishizawa, N. Mizutani, M. Kato, J. Ceram. Soc. Jpn. 93 (1985) 649.
[18] D.M. Gruen, W.C. Koehler, J.J. Katz, J. Am. Chem. Soc. 73 (1951) 1475.
[19] V. Perrichon, A. Laachir, G. Bergeret, R. Frety, T. Louise, O. Touret, J. Chem. Soc. Faraday Trans. 90 (1994) 773.
[20] A.B. Hungría, PhD Thesis, Univ. Complutense de Madrid, 2004.
[21] (a) T.X.T. Sayle, S.C. Parker, C.R.A. Catlow, J. Chem. Soc. Chem. Commun. (1992) 977;
(b) J.C. Conesa, Surf. Sci. 339 (1995) 337.
[22] P. Fornasiero, T. Montini, M. Graziani, J. Kašpar, A.B. Hungría, A. Martínez-Arias, J.C. Conesa, Phys. Chem. Chem. Phys. 4 (2002) 149.
[23] R.C. Karnatak, J. Alloys Compd. 192 (1993) 64.
[24] G. Blanco, J.M. Pintado, S. Bernal, M.A. Cauqui, M.P. Corchado, A. Galtayries, J. Ghijsen, R. Sporken, T. Eickhoff, W. Drube, Surf. Interface Anal. 34 (2002) 120.
[25] G. Munuera, in preparation.
[26] D.M. Gruen, W.C. Koehler, J.J. Katz, J. Am. Chem. Soc. 73 (1951) 1475.
[27] V.V. Kharton, F.M.B. Marques, A. Atkinson, Solid State Ionics 174 (2004) 135.
[28] V.V. Kharton, F.M. Figueiredo, L. Navarro, E.N. Naumovich, A.V. Kovalevsky, A.A. Yaremchenko, A.P. Viskup, A. Carneiro, F.M.B. Marques, J.R. Frade, J. Mater. Sci. 36 (2001) 1105.